Supporting Information

Synergy of intramolecular hydrogen bonding and π-bridge locking enables high-efficiency red/NIR electroluminescence

Hui Wang[a], Chuan-Sheng Ping[a], Chen-Long Lou[a], Jia Yu[ab], Xiao-Chun Fan[ab]*, Kai Wang[ac]*

[a.] Institute of Functional Nano & Soft Materials (FUNSOM), Soochow University, Suzhou, Jiangsu 215123, P. R. China.
[b.] Jiangsu Key Laboratory of Advanced Negative Carbon Technologies, Soochow University, Suzhou, 215123, Jiangsu, PR China.
[c.] State Key Laboratory of Bioinspired Interfacial Materials Science, Soochow University, Suzhou, 215123, Jiangsu, PR China.

Email: xcfan@suda.edu.cn, wkai@suda.edu.cn.

General information

Materials. All commercially available reagents were used as received unless otherwise stated. All reactions were carried out using Schlenk techniques under a nitrogen atmosphere. ^{1}H and ^{13}C NMR spectra were measured on a Bruker 400 MHz spectrometer with tetramethylsilane (TMS) as the internal standard. Mass analyses were recorded by an Autoflex MALDI-TOF mass spectrometer.

Theoretical calculation. The optimized structures, distributions of HOMO and LUMO, excited states levels and Natural transition orbitals (NTOs) of the lowest adiabatic excited states were analyzed by B3LYP/6-31g (d) basis set via a multifunctional wavefunction analyzer (Multiwfn 3.7). The reorganization energies consist of the external and internal reorganization energy. The external reorganization energy caused by the polarization of the medium can be negligible. The internal reorganization energy is caused by the geometrical deformation in the Franck–Condon vertical absorption transition and radiative process, and the value can be estimated as the following equation:

$$\lambda = \lambda_{S_0} + \lambda_{S_1} = \left[E^{S_0}(S_1) - E^{S_0}(S_0) \right] + \left[E^{S_1}(S_0) - E^{S_1}(S_1) \right] \quad \text{(S1)}$$

Here, $E^{S_0}(S_1)$ is the energy of the S_0 state with the optimized S_1 geometry, $E^{S_0}(S_0)$ is the energy of the S_0 state with the optimized S_0 geometry, $E^{S_1}(S_0)$ is the energy of S_1 state with the optimized S_0 geometry, and $E^{S_1}(S_1)$ is the energy of S_1 state with the optimized S_1 geometry. The single point energy was calculated at B3LYP level with 6-31G (d, p) basis set. The decomposition of the reorganization energies was realized by using Gaussian 16 software package. The spin-density distributions (SSDs) of the lowest excited triplet states were analyzed using a multifunctional wavefunction analyzer (Multiwfn 3.7) and visualized with VMD program.

Electrochemical and thermal measurements. Cyclic voltammetry was performed on a CHI 660 instrument. Individual samples were dissolved in dichloromethane solution and degassed with nitrogen gas for 15 minutes before the test. 0.1 M tetrabutylammonium perchlorate in 10^{-3} M dichloromethane (DCM) solution served as

the supporting electrolyte with ferrocene/ferrocenium (Fc/Fc+) as the internal reference. A saturated silver chloride (AgCl) electrode, Pt disks and gold (Au) electrode were used as a reference electrode, counter electrode and working electrode, respectively. The energy levels of HOMO (E_{HOMO}) and LUMO (E_{LUMO}) of the compounds were determined from onset position of their oxidation and reduction curves in 10^{-3} M DCM solution relative to that of Fc^{+}/Fc by using the equations E_{HOMO} (eV) = $-(E_{ox} - E_{1/2,\ Fc} + 5.1)$ eV and E_{LUMO} (eV) = $-(E_{re} - E_{1/2,\ Fc} + 5.1)$ eV. Thermogravimetric analysis (TGA) was performed on a TA SDT 2960 instrument at a heating rate of 10 °C min^{-1} under nitrogen. Temperature at 5% weight loss was used as the decomposition temperature (T_d).

Photophysical measurements. UV–Vis absorption spectra were recorded on a Hitachi U-3900 spectrophotometer. PL spectra were recorded on a Hitachi F-4600 fluorescence spectrophotometer with default collection intervals. Transient fluorescence decays were measured with a Quantaurus-Tau fluorescence lifetime spectrometer (C11367-32, Hamamatsu Photonics) with an excitation wavelength of 373 nm and pulse width of 100 ps. The absolute PL quantum yields were recorded on a Hamamatsu Quantaurus-QY quantum yield spectrometer (C13534-11).

Single-Crystal Structure. Diffraction data were collected on a Rigaku R-AXIS-RAPID diffractometer using ω-scan mode with graphite-monochromator MoKα radiation. The structure determination was solved with direct methods using the SHELXTL programs and refined with full-matrix least squares on F^2. All crystallographic information in CIF format has been deposited at the Cambridge Crystallographic Center (CCDC) under deposition number 2175310 for QCN-AC via www.ccdc.cam.ac.uk/data_request/cif.

Device fabrication and measurement of EL characteristics. All the emitters were applied in the OLEDs after sublimation. OLEDs were fabricated on the indium-tin oxide (ITO) coated transparent glass substrates. Before device fabrication, the substrates were cleaned with ethanol, acetone and deionized water, and then dried in an oven, finally exposed to UV ozone for 15 min. All the organic materials and metal layers were thermal evaporated under a pressure of 4 ß 10^{-4} Pa. EL spectra, luminance,

efficiency and current density–voltage–luminance characteristics were measured with a constant-source Keithley 2400 source meter and an integrating sphere (Hamamatsu C9920-02).

Experimental

Synthesis

2-(4-Bromophenyl)quinoxaline-6,7-dicarbonitrile (**QCN-Br**) and **QCN-TPA** were synthesized according to a previous report.[1] The intermediate product 9,9-dimethyl-10-phenyl-2-(4,4,5,5-tetramethyl-1,3,2-dioxaborolan-2-yl)-9,10-dihydroacridine (**AC-Bpin**) was also obtained according to the reported literature.[2]

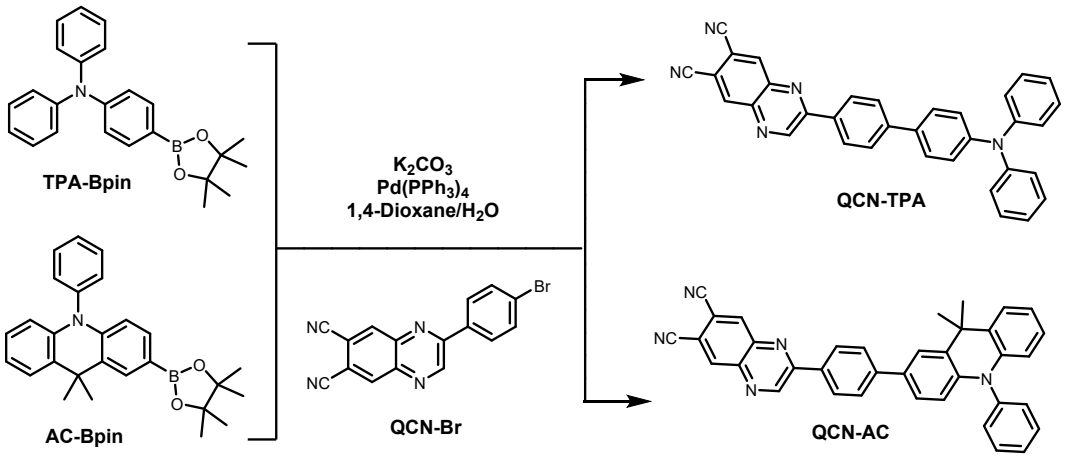

Scheme S1. Experimental procedure of **QCN-TPA** and **QCN-AC**.

2-(4-(9,9-Dimethyl-10-phenyl-9,10-dihydroacridin-2-yl)phenyl)quinoxaline-6,7-dicarbonitrile (QCN-AC)

QCN-Br (1.00 g, 3 mmol), AC-Bpin (1.35 g, 3.3 mmol), K_2CO_3 (0.85 g, 6 mmol), $Pd(PPh_3)_4$ (174 mg, 0.15 mmol) and 80 mL of 1,4-dioxane/H_2O (1:1) were added to a three-necked flask (100 mL) under a nitrogen atmosphere. Then, the mixture was stirred at 100 °C for 24 h. After the reaction was completed, dichloromethane and water were added, and the organic layer was separated and concentrated in vacuo. The solid residue

was purified by column chromatography with dichloromethane to obtain the product (1.00 g, 62%). ^{1}H NMR (400 MHz, $CDCl_3$, δ): δ 9.57 (s, 1H), 8.60 (d, J = 11.8 Hz, 2H), 8.33 (d, J = 8.5 Hz, 2H), 7.83–7.79 (m, 3H), 7.67 (t, J = 7.7 Hz, 2H), 7.56 (t, J = 7.5 Hz, 1H), 7.50 (dd, J = 7.4, 1.9 Hz, 1H), 7.39–7.36 (m, 2H), 7.32 (dd, J = 8.6, 2.2 Hz, 1H), 6.99 (td, J = 7.0, 1.7 Hz, 2H), 6.39 (d, J = 8.6 Hz, 1H), 6.32–6.29 (m, 1H), 1.79 (s, 6H). m/z: [M]+ Calcd for $C_{37}H_{25}N_5$, 539.31; found, 539.35.

Theoretical calculations

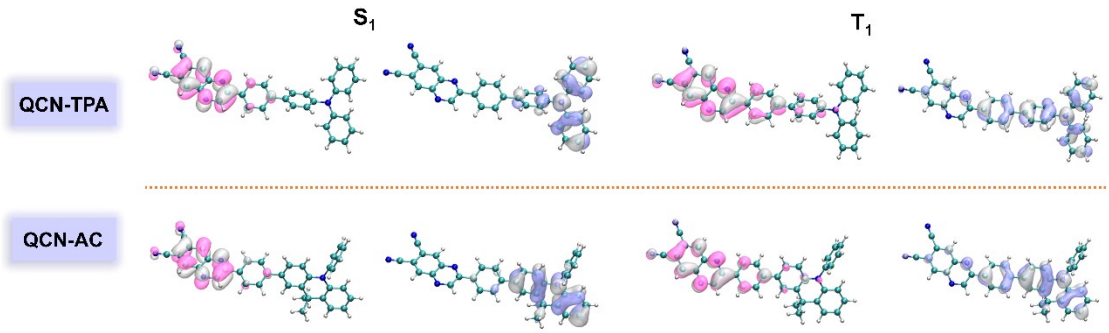

Fig. S1 Natural transition orbital (NTO) analysis of **QCN-TPA** and **QCN-AC**.

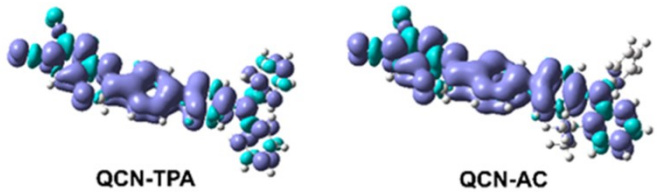

Fig. S2 Triplet spin density distribution (SDD) analysis of **QCN-TPA** and **QCN-AC**.

Table S1. Summary of the theoretical calculated results of **QCN-TPA** and **QCN-AC**.

Molecule	HOMO (eV)	LUMO (eV)	E_g (eV)	S_1 (eV)	T_1 (eV)	ΔE_{ST} (eV)	f
QCN-TPA	-5.24	-2.94	2.39	2.04	1.86	0.18	0.27
QCN-AC	-5.16	-2.89	2.26	2.02	1.82	0.20	0.29

Electrochemical properties

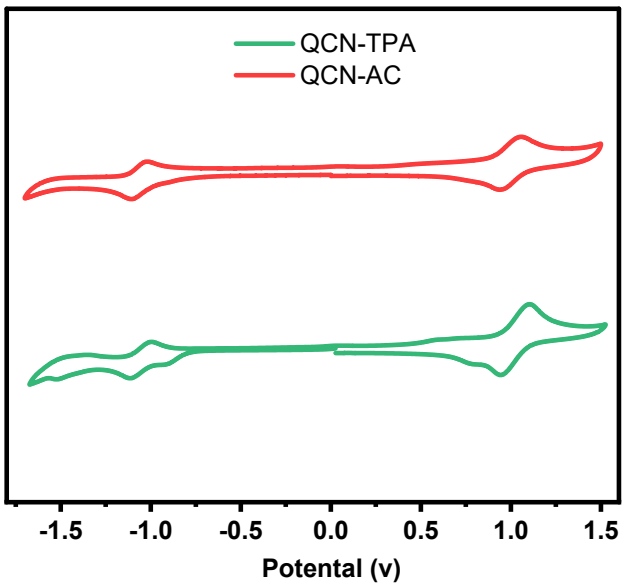

Fig. S3 Cyclic voltammogram curves of **QCN-TPA** and **QCN-AC**.

Thermal properties

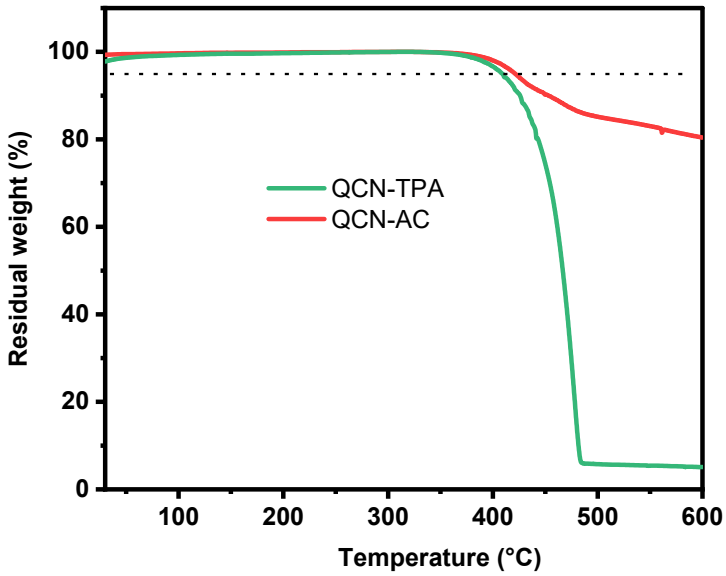

Fig. S4 TGA curves of **QCN-TPA** and **QCN-AC**.

Transient PL measurements

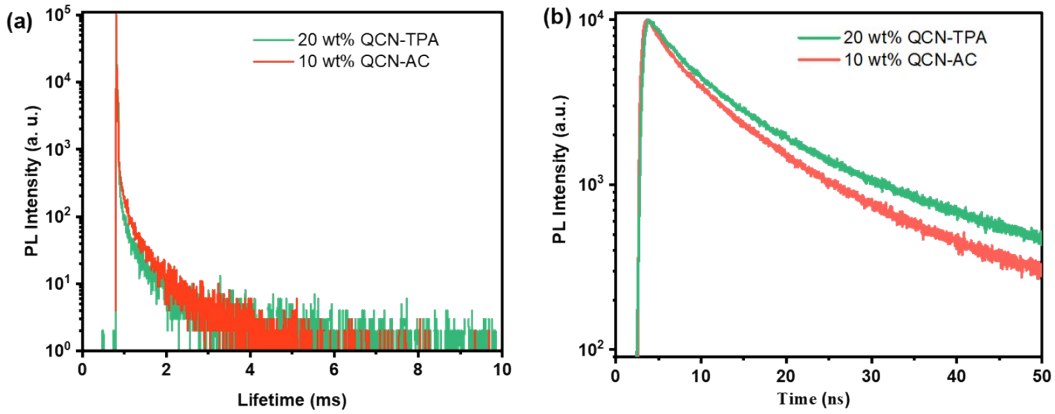

Fig. S5 Transient PL decay curves of 20 wt% **QCN-TPA**, 10 wt% **QCN-AC** doped in CBP films in the time range of (a) 10 ms and (b) 50 ns at 300 K under vacuum conditions.

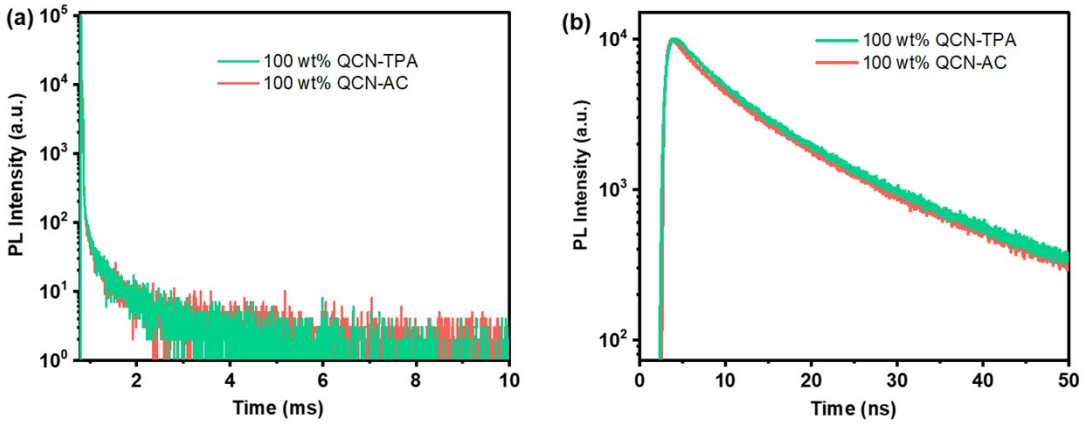

Fig. S6 Transient PL decay curves of neat films based on **QCN-TPA** and **QCN-AC** measured at 300 K under vacuum, with time scales of (a) 10 ms and (b) 50 ns.

Table S2. Kinetic parameters of **QCN-TPA** and **QCN-AC**.

EMLs	wt [%]	ϕ_{PL} [%]	ϕ_P/ϕ_d [%]	τ_p [ns]	τ_d [μs]	k_r^s [10^7 s^{-1}]	k_P [10^7 s^{-1}]	k_d [10^5 s^{-1}]	k_{ISC} [10^7 s^{-1}]	k_{RISC} [10^5 s^{-1}]	k_{IC} [$10^7 s^{-1}$]
QCN-TPA	20	80	27/53	13.4	347	2.0	7.4	2.9	5.4	7.6	0.5
	100	20	12/8	15.8	471	0.7	6.3	2.1	5.6	1.8	2.8
QCN-AC	10	98	50/48	10.7	404	4.6	9.3	2.5	4.7	4.8	0.09
	100	25	8/17	11.8	574	0.7	8.5	1.7	7.8	3.9	2.1

Table S3. Crystal data and structure refinement for **QCN-AC.**

Identification code	QCN-AC
Empirical formula	$C_{37}H_{25}N_5$
Formula weight	539.62
Temperature/K	170
Crystal system	triclinic
Space group	P-1
a/Å	7.5549(9)
b/Å	11.1032(12)
c/Å	17.0569(18)
α/°	88.391(4)
β/°	89.786(4)
γ/°	77.616(4)
Volume/Å^3	1396.9(3)
Z	2
ρ_{calc}g/cm^3	1.283
μ/mm^{-1}	0.077
F(000)	564.0
Crystal size/mm^3	0.15 × 0.08 × 0.05
Radiation	MoKα (λ = 0.71073)
2Θ range for data collection/°	3.758 to 52.9

Index ranges	$-9 \le h \le 9, -13 \le k \le 13, -21 \le l \le 21$
Reflections collected	15829
Independent reflections	5682 [R_{int} = 0.0869, R_{sigma} = 0.1160]
Data/restraints/parameters	5682/0/381
Goodness-of-fit on F^2	1.011
Final R indexes [I>=2σ (I)]	R_1 = 0.0764, wR_2 = 0.1684
Final R indexes [all data]	R_1 = 0.1817, wR_2 = 0.2285
Largest diff. peak/hole / e $Å^{-3}$	0.29/-0.25

Electroluminescence properties

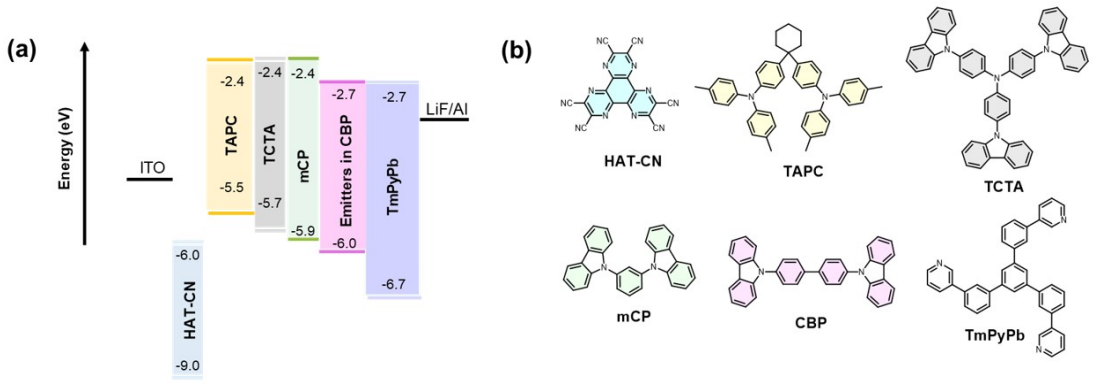

Fig. S7 (a) Device structure and (b) materials used in the OLED devices.

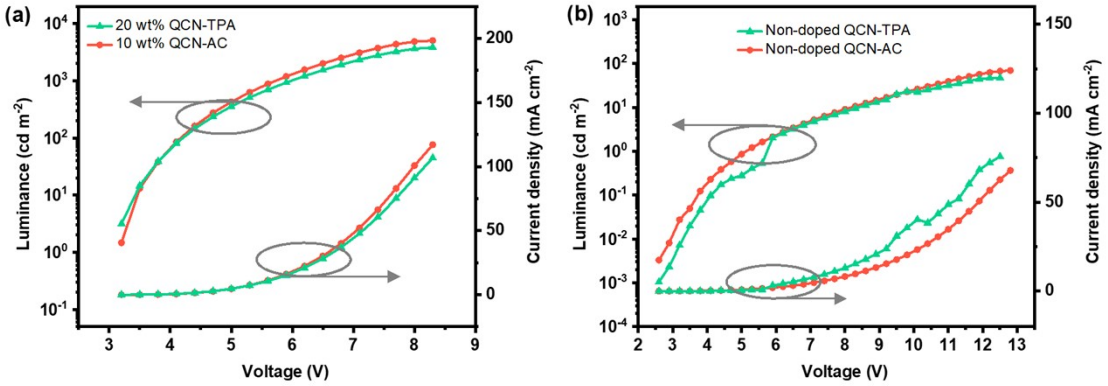

Fig. S8 J–V–L curves of **QCN-TPA** and **QCN-AC** for (a) doped devices and (b) nondoped devices.

Table S4. EL performances of the OLED devices based on **QCN-TPA** and **QCN-AC** at various doping ratios.

Emitters	wt (%)	Peak (nm)	CE_{max} (cd A^{-1})	PE_{max} (lm W^{-1})	EQE_{max} (%)	CIE (x, y)
QCN-TPA	5	592	30.8	25.4	13.6	(0.54, 0.45)
	10	612	22.8	22.3	14.4	(0.59, 0.40)
	15	616	21.0	17.8	14.9	(0.60, 0.40)
	20	620	24.6	24.1	16.8	(0.60, 0.39)
	30	644	11.0	10.7	13.5	(0.64, 0.35)
	100	748	0.06	0.12	1.85	(0.70, 0.30)
QCN-AC	5	604	47.8	51.8	23.6	(0.57, 0.43)
	10	620	43.8	43.0	29.6	(0.60, 0.40)
	15	632	27.6	22.2	22.9	(0.63, 0.36)
	20	640	15.7	15.4	16.8	(0.64, 0.35)
	30	652	7.6	7.4	12.6	(0.66, 0.33)
	100	744	0.11	0.14	3.18	(0.70, 0.30)

NMR Spectra

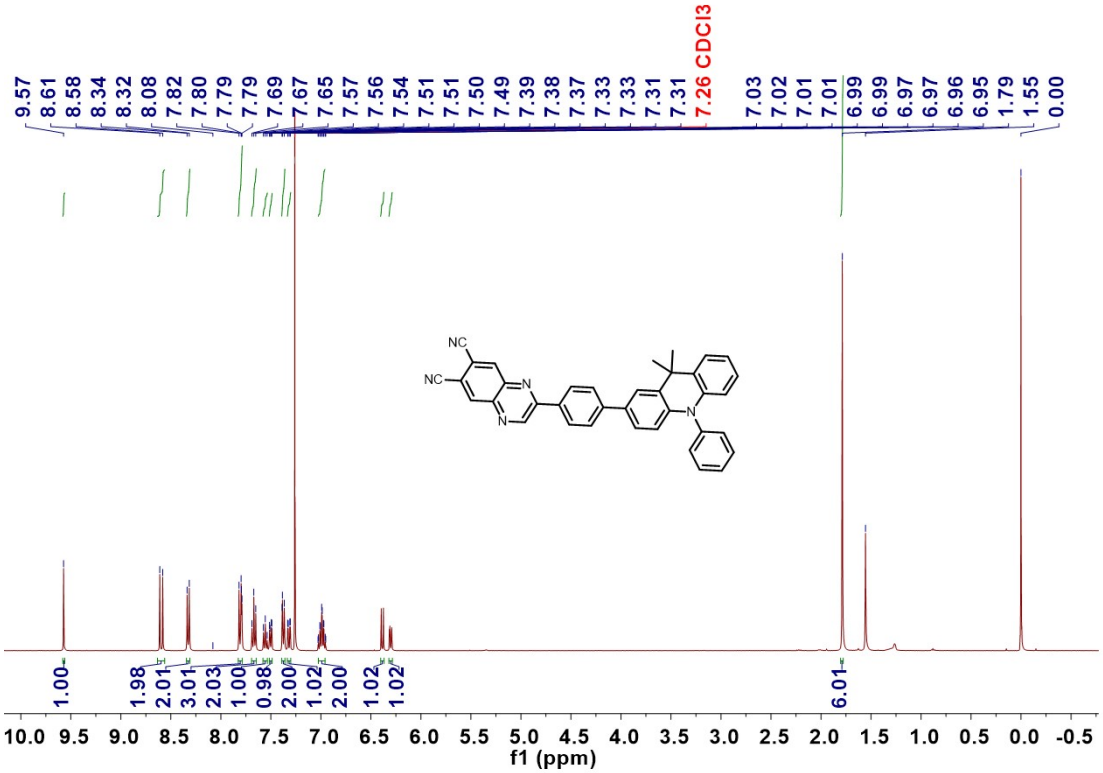

Fig. S9 ^{1}H NMR spectrum ($CDCl_3$, 400 MHz) of **QCN-AC**.

References

[1] C. Li, R. Duan, B. Liang, G. Han, S. Wang, K. Ye, Y. Liu, Y. Yi, Y. Wang, *Angewandte Chemie International Edition*, 2017, **56**, 11525-11529.

[2] Y.-K. Wang, C.-C. Huang, S. Kumar, S.-H. Li, Z.-L. Dong, M.-K. Fung, Z.-Q. Jiang, L.-S. Liao, *Journal of Materials Chemistry C*, 2018, **6**, 10030-10035.